Electronic Supplementary Information (ESI)

Modulation of mechanical properties and stable light energy harvesting by poling in polymer integrated perovskite films: A wide range, linear and highly sensitive tactile sensor

Rohit Saraf[a], Ting Tsui*[b] and Vivek Maheshwari*[a]

[a]*Department of Chemistry, Waterloo Institute for Nanotechnology, University of Waterloo, Waterloo, ON N2L 3G1, Canada*
[b]*Department of Chemical Engineering, Waterloo Institute for Nanotechnology, University of Waterloo, Waterloo, ON N2L 3G1, Canada*

**E-mail: vmaheshwari@uwaterloo.ca, tttsui@uwaterloo.ca*

EXPERIMENTAL SECTION

***Materials*:** Methylamine (CH_3NH_2), hydroiodic acid (HI), lead iodide (PbI_2), polystyrene (PS), N,N-dimethylformamide (DMF), dimethyl sulfoxide (DMSO), diethyl ether, anhydrous zinc chloride ($ZnCl_2$), and potassium chloride (KCl) were all purchased from Sigma-Aldrich and no further purification was required.

***CH_3NH_3I precursor synthesis*:** The methylammonium iodide (CH_3NH_3I, MAI) precursor was synthesized through the reaction of HI with CH_3NH_2 followed by recrystallization from ethanol. An equimolar amount of HI (57 wt % in water) was added dropwise into the CH_3NH_2 (33 wt % in absolute ethanol) under constant stirring at 0 °C for 2 h. A dark yellow precipitate was obtained by removing the solvent using a rotary evaporator. The precipitate was then washed with diethyl ether (several times) and recrystallized with ethanol. The white MAI powder was dried in vacuum overnight.

***$MAPbI_3$ and PS-$MAPbI_3$ precursor solutions preparation*:** The $MAPbI_3$ precursor solution (1.35 M) was prepared by dissolving PbI_2, MAI, and DMSO (molar ratio = 1:1:1) in anhydrous DMF. The 1wt %, 3 wt %, and 7 wt % PS-$MAPbI_3$ precursor solutions were prepared by first dissolving the required amount of PS in DMSO (53.3 μL) and DMF (317.5 μL). Then, MAI and PbI_2 (1/1 by molar) were added to the above PS solution with a constant stirring for 1 h (time for crosslinking) at room temperature.

***Perovskite thin film fabrication*:** The silicon chips with a dimension of 1.3 cm × 1.3 cm patterned with gold electrodes were fabricated on the top of 200 nm thick SiO_2 layer by photolithography with a Cr adhesion layer. At the center of the chip, the alternating fingers form the Au positive electrode and the Au ground (negative) electrode with an electrode spacing of 2 μm. The patterned Au chips were cleaned in an ultra-sonication bath in acetone, isopropyl alcohol, and water for 20 min, respectively. The chips were then treated by piranha solution to remove trace amounts of organic residues and to make the surface hydrophilic for ensuring proper wetting by the perovskite film. Then, the chips were washed thoroughly with the

Millipore water and dried by an air gun. The $MAPbI_3$ or PS-$MAPbI_3$ precursor solution was spun on a cleaned Au chip at 4000 rpm for 30 s. After 8 s of rotation, the diethyl ether was dropped onto the center of the Au chip. Thereafter, the chip was annealed at 65 °C for 2 min and 100 °C for 3 min.

***Electrochemical deposition of ZnO nanosheets*:** The electrochemical deposition of ZnO nanosheets was performed using an Ivium potentiostat in a three-electrode electrochemical cell. The Indium tin oxide (ITO) coated glass substrate as the working electrode, a platinum wire as the counter electrode and an Ag/AgCl electrode as the reference electrode. ITO glass substrate (R_s = 8-12 Ω/sq) was purchased from Delta Technologies. ITO glass substrates were cleaned in acetone, isopropanol, and Millipore water by ultra-sonication for 15 min, respectively. The electrolyte was an aqueous solution of 28 mM $ZnCl_2$ and 0.1 M KCl. The ZnO nanosheets were electrodeposited at 70 °C under a constant potential of -1.035 V for 1 h. After deposition, the substrate was gently washed with Millipore water and annealed at 335 °C for 1 h.

***Film characterization*:** A ZEISS Ultraplus Field emission scanning electron microscopy (FESEM) was used to study the morphology of the perovskite films and ZnO nanosheets. A glancing incidence X-ray diffraction (GIXRD) patterns were measured on PANalytical X'Pert Pro MRD diffractometer utilizing a Cu Kα radiation at an incidence angle of 0.4°. A Horiba HR800 spectrometer in the backscattering configuration was used to measure the Raman spectra. The excitation wavelength of the laser was 532 nm and the power was 0.6 mW to avoid any sample degradation effects. For measuring the molecular weight of cross-linked polystyrene within $MAPbI_3$, gel permeation chromatography (GPC) was employed. Samples dissolved in THF were injected into a Viscotek VE 2001 GPC instrument equipped with PolyAnalytik SupeRes mixed bed columns, TDA 305 triple detector array and a 2600 UV detector, using THF as the eluent. The columns were maintained at a temperature of 35 °C and the flow rate was 1 mL min^{-1}. The elastic modulus and hardness were measured using an in situ

nanoindenter (Nanomechanics Inc. Knoxville, TN) equipped with a dynamic control module and a sharp Berkovich diamond tip. Harmonic displacement and frequency was targeted at 1 nm and 75 Hz respectively. Thin film specimen Poisson's ratio was assumed to be 0.25. Experiments were performed when the instrument thermal drift rate was less than 0.05 nm/s. Data were analyzed according to the Oliver and Pharr model.[1] Area function was validated with a fused silica specimen at indentation depths in the range of 50 and 300 nm.

***Device measurement*:** Simulated AM 1.5G irradiation (10 mW cm^{-2}) with a xenon-lamp based solar simulator (Newport Oriel Instrument 67005, 150W Solar Simulator) was used as the illumination source. The light intensity was calibrated before photocurrent measurement by a silicon (Si) diode (Hamamatsu S1133) equipped with a Schott visible-color glass-filtered (KG5 color-filtered) to minimize spectral mismatch. A black box was used to avoid stray light. The probing station was used to conduct the measurements on the symmetric lateral Au/PS-$MAPbI_3$ (or $MAPbI_3$)/Au structure cell configuration. The plain $MAPbI_3$ or PS-$MAPbI_3$ films were poled at different voltages for 5 min, by connecting one probe to the Au pad on the Au chip and another probe connected to the Au ground. The poling was done under 0.1 sun illumination and in ambient atmosphere (presence of O_2) to generate an internal polarization (ferroelectric effect) in the films. A Keysight 6614C 50 Watt system power supply with a maximum voltage output of 100 V was used for the poling process. After poling the device, the short circuit current density (J_{sc}) and the open circuit voltage (V_{oc}) were recorded using a Keysight 3458A Digital multimeter. The film was connected in series with the multimeter and power supply to form a circuit. For measuring the power (or energy) density of the plain $MAPbI_3$ and PS-$MAPbI_3$ films, first the film was electrically poled at a particular voltage for 5 min and then the J_{sc} was recorded as a function of external load resistance. For the self-powered tactile sensor, ZnO nanosheets on ITO substrate were used as the top sample and Au/PS-$MAPbI_3$ (or $MAPbI_3$)/Au lateral structure was used as the bottom sample. First, the PS-$MAPbI_3$ (or $MAPbI_3$) film was poled under 0.1 sun illumination in an ambient atmosphere and then the

ZnO nanosheets were interfaced with the perovskite layer. Three probes system was used; the first probe was connected to the Au pad, the second probe was connected to the Au ground electrode on Au chip, and the third probe was connected to the ITO substrate. An MFA Motorized Miniature Linear Stage was used to apply the pressure load to the samples. A Honeywell Model 31 Miniature Load Cell was connected to the stage for measuring the load. Combined with a micro-pro series digital panel meter, we were able to read out the measurements and record the data. The operational stability and continuous power generation from the 1 wt % PS-$MAPbI_3$ device (with or without the ZnO interface) was carried out in an ambient environment by initially poling the device for 5 min (under 0.1 sun illumination and in ambient air), and then tracking the J_{sc} response by applying an external load resistance identical to the resistance at maximum power point (R_{MPP}) in the current-resistance curves. During measurements, the devices were maintained at a constant resistance (R_{MPP}) and subjected to continuous 0.1 sun, AM 1.5G illumination in ambient air with 40–50% relative humidity. All measurements were conducted in an ambient air without device encapsulation.

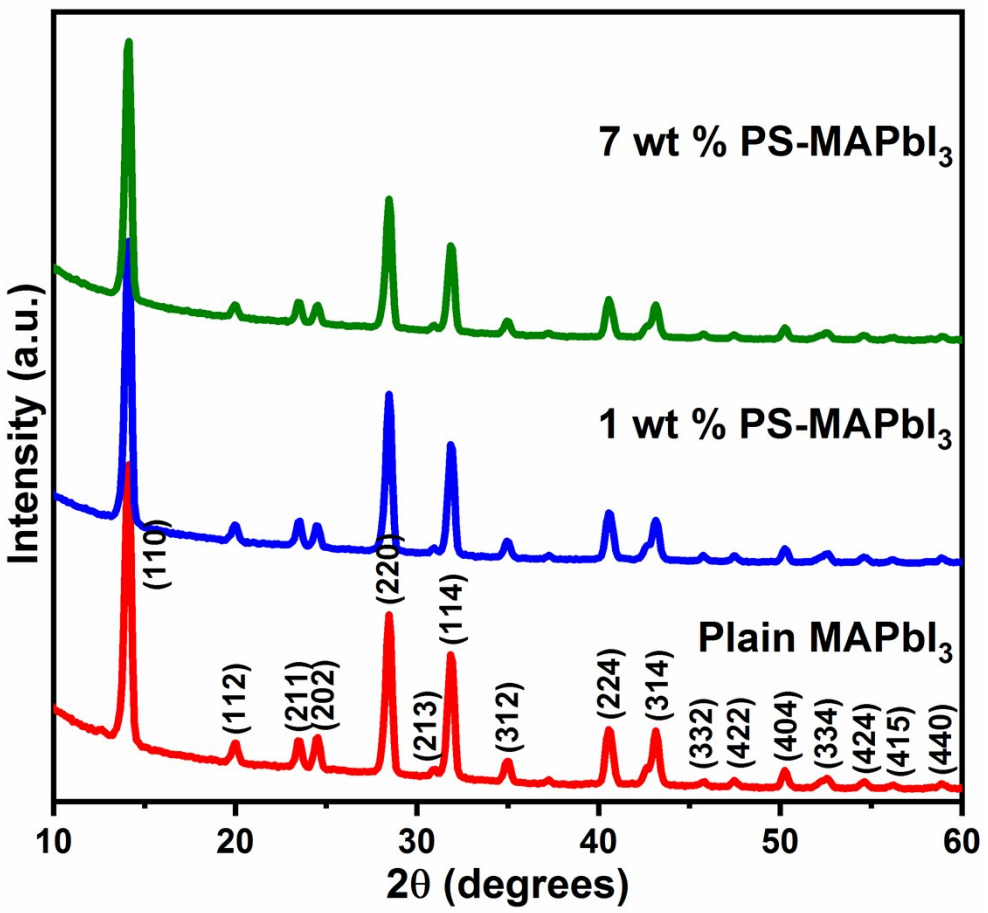

Fig. S1. X-ray diffraction patterns of plain $MAPbI_3$, 1 wt %, and 7 wt % PS-$MAPbI_3$ films.

The crystal structure of the perovskite films was examined by conducting the glancing incidence XRD measurements. All the samples show the same tetragonal perovskite phase with the dominant (110) lattice plane.

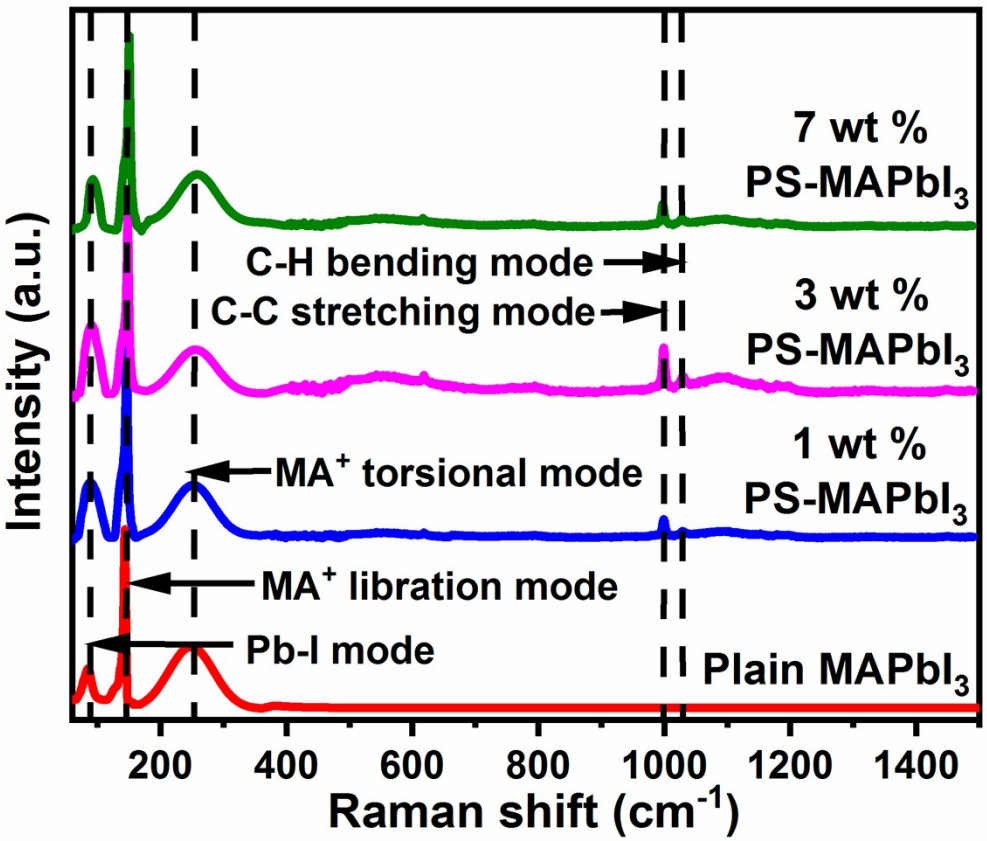

Fig. S2. Raman spectra of plain $MAPbI_3$, 1 wt %, 3 wt %, and 7 wt % PS-$MAPbI_3$ films.

The sharp characteristic Raman peaks observed at 84 cm^{-1} and 143 cm^{-1} in plain $MAPbI_3$ can be assigned to the Pb–I and MA^+ libration modes, respectively. The broad band with maxima around 247 cm^{-1} attributed to the MA^+ torsional mode in the plain $MAPbI_3$. The shift of the Pb–I, MA^+ libration, and MA^+ torsional modes from 84 to 92 cm^{-1}, 143 to 150 cm^{-1}, and 247 to 258 cm^{-1}, respectively with the increase in the PS content to 7 wt % is indicative of the interaction of PS with Lewis acid PbI_2 and MA^+ cations. This interaction leads to the formation of an intermediate PS-PbI_2 and PS-MA^+ adducts, which will improve the crystallinity of the perovskite films. Further, we also observed the stretching vibration of C–C aromatic in 1 wt %, 3 wt %, and 7 wt % PS-$MAPbI_3$ at 998 cm^{-1}. The bending vibration of C–H aromatic in all PS-$MAPbI_3$ films appears at 1030 cm^{-1}. Both the stretching and bending vibrations observed in PS-$MAPbI_3$ films reflect the incorporation of PS into $MAPbI_3$.

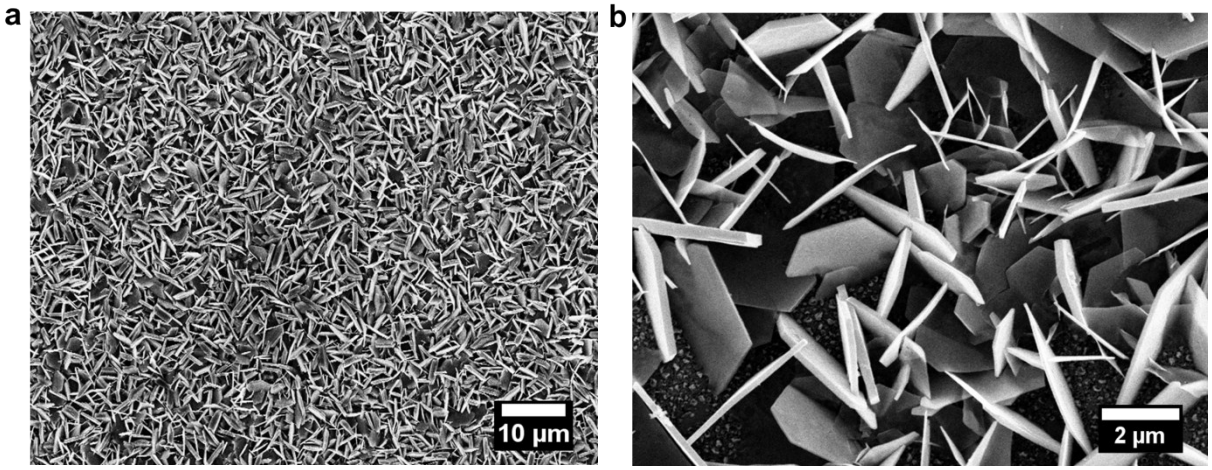

Fig. S3. Field emission scanning electron microscopy (FESEM) images of electrochemically-deposited ZnO nanosheets.

The lower resolution image (Fig. S3a) shows the high density of the ZnO nanosheets on the ITO substrate. The higher resolution image (Fig. S3b) reveals that the average sheet size is 3 μm with a thickness on the scale of 50–150 nm.

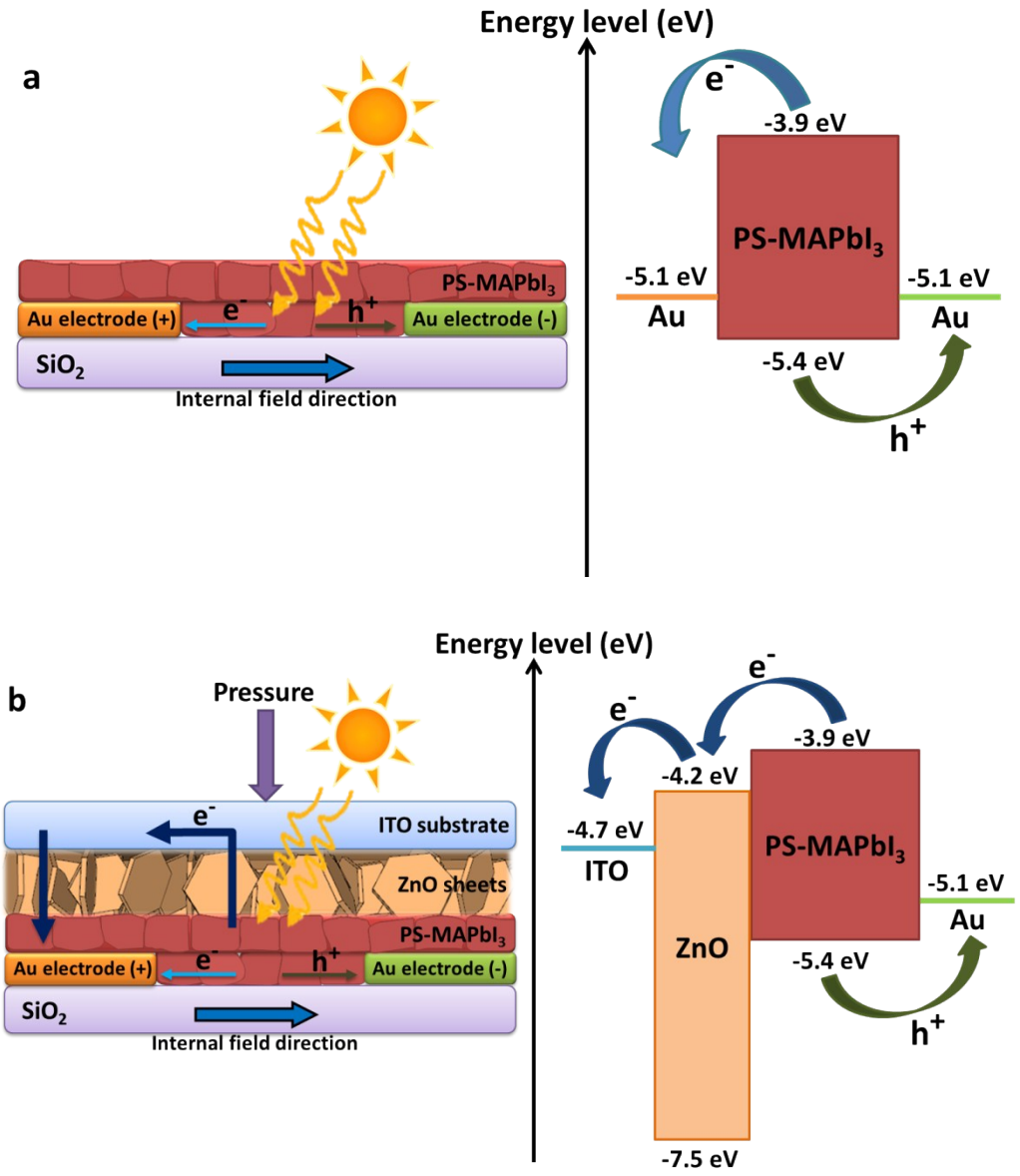

Fig. S4. Energy level diagram of the PS-MAPbI$_3$ device a) Without ZnO (Au/PS-MAPbI$_3$/Au), and b) With ZnO (ITO/ZnO/PS-MAPbI$_3$/Au).

When the light is illuminated on the device, the photo-generated charge carriers (electrons and holes) in PS-MAPbI$_3$ layer will separate under the polarization field. In the symmetric device configuration (Au/PS-MAPbI$_3$/Au) as shown in Fig. S4a, the work function of Au closely matches with the PS-MAPbI$_3$ perovskite Highest Occupied Molecular Orbital (HOMO) which leads to favorable hole collection by the negative gold electrode. Whereas, the electrons are not easily collected by the positive Au electrode due to the large difference in the energy level of PS-MAPbI$_3$ LUMO (Lowest Unoccupied Molecular Orbital) and Au. By

interfacing the ZnO sheets with the PS-$MAPbI_3$ film (Fig. S4b), the electron extraction efficiency will improve due to the matching of the energy level of PS-$MAPbI_3$ LUMO with the ZnO LUMO and hence leads to increased J_{sc}. In the absence of external pressure, the vertically oriented microstructured ZnO sheets have a limited area of interaction with the PS-$MAPbI_3$ layer. When the pressure is applied, the contact area of ZnO sheets with the PS-$MAPbI_3$ film will increase either due to bending or penetration of the ZnO sheets. The increase in an interfacing area will improve the charge collection, which facilitates the pressure-sensitive modulation in J_{sc}.

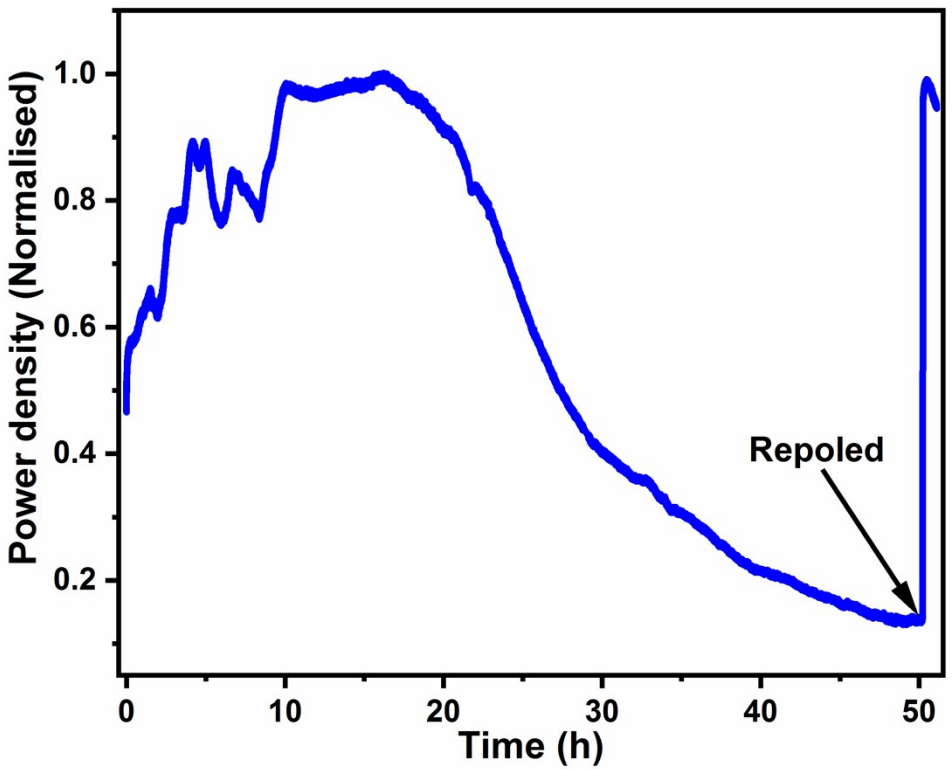

Fig. S5. Operational stability and continuous power generation test for the 1 wt % PS-$MAPbI_3$ device (after 5 V/μm poling) without ZnO interface, examined at maximum power point with a constant resistance of 20 MΩ under continuous 0.1 sun illumination in air.

The 1 wt % PS-$MAPbI_3$ device (without ZnO layer) after poling for just 5 min generate stable and continuous power density for more than 24 h. We observed a decrease in the power density with time due to the depolarization of the films and not to any structural degradation. This is confirmed by repoling the device at 5 V/μm for 5 min and subsequently the efficiency is recovered.

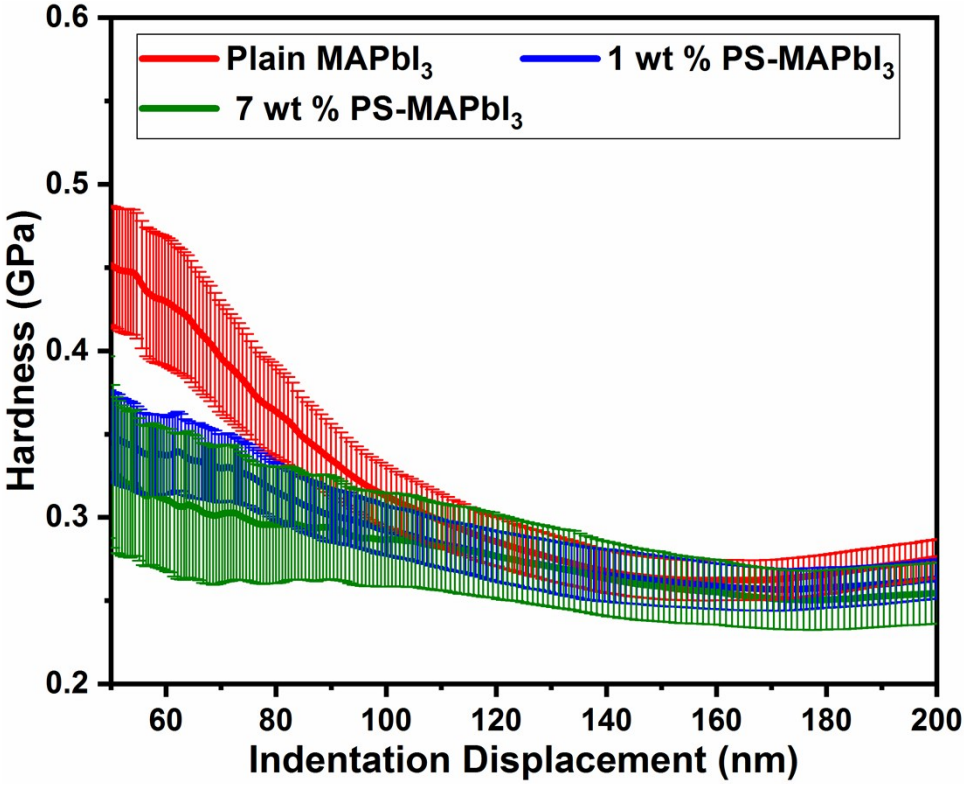

Fig. S6. Hardness of plain $MAPbI_3$, 1 wt %, and 7 wt % PS-$MAPbI_3$ films.

The average hardness value for plain $MAPbI_3$ films at indentation depth of 75 nm is found to be 0.38 GPa. It can be clearly observed that this value reduces to 0.33 GPa, and 0.30 GPa as the PS content in the precursor solution is increased to 1 wt %, and 7 wt %, respectively. This reveals that the increment in the wt % of PS in the precursor solution leads to the formation of softer films, which allows us to tune the dynamic pressure range of the sensors.

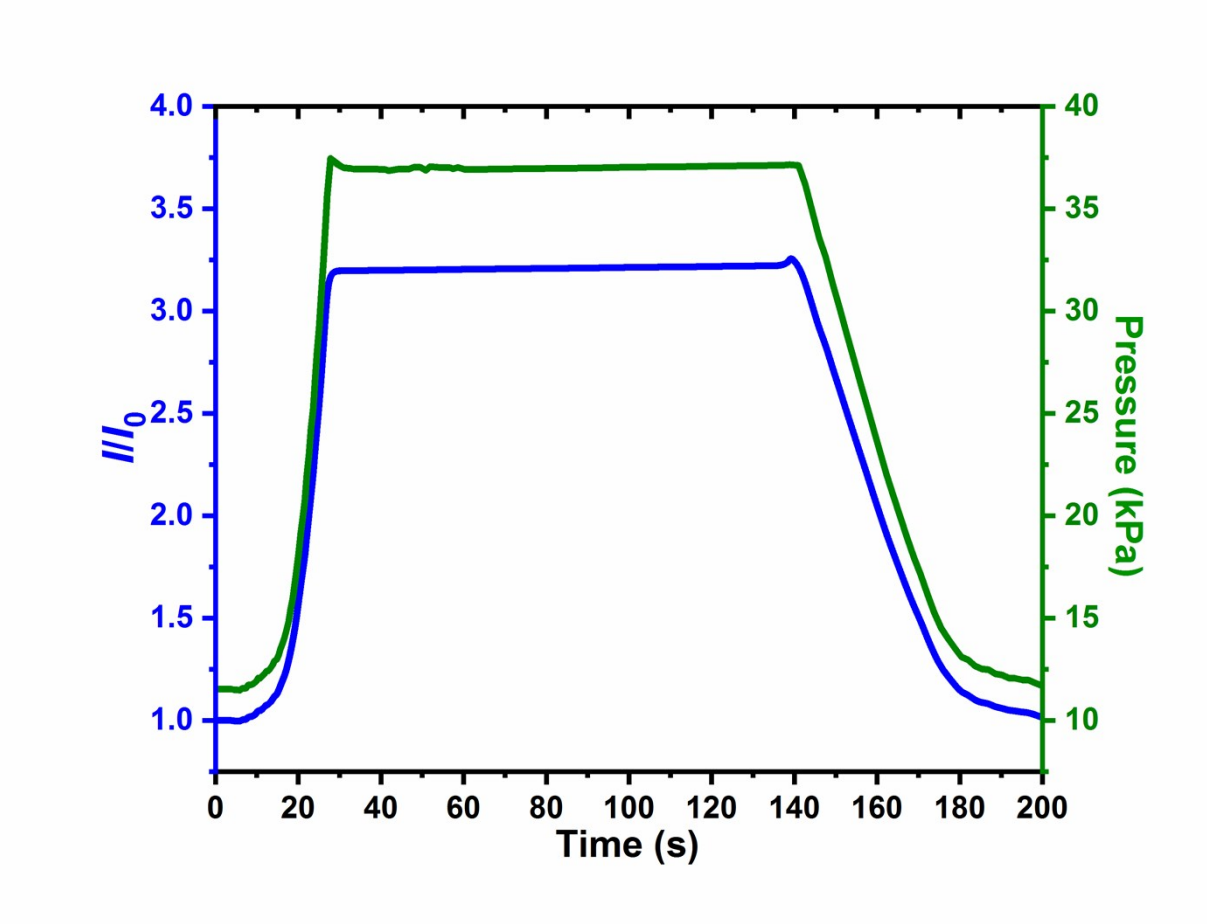

Fig. S7. Relative current (I/I_0) for plain $MAPbI_3$ device increases with the increase in pressure from 0 kPa to 37 kPa and is maintained constant under a constant load.

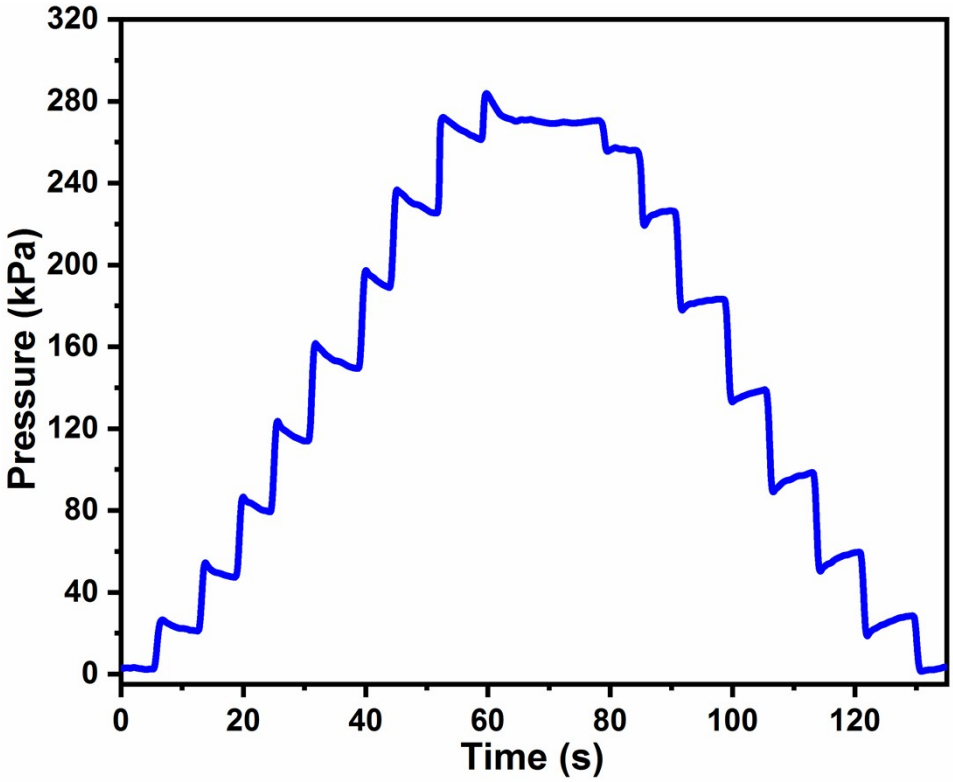

Fig. S8. Pressure curves as a step function recorded using two glass slides.

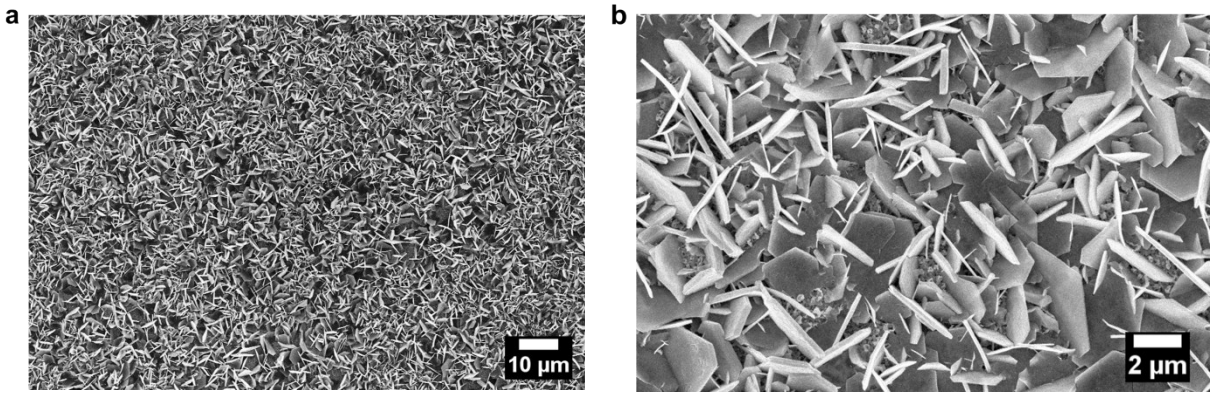

Fig. S9. FESEM images of the ZnO sheets after 100 load cycles of 200 kPa pressure shows no change in the morphology, thus confirming the stability of the device.

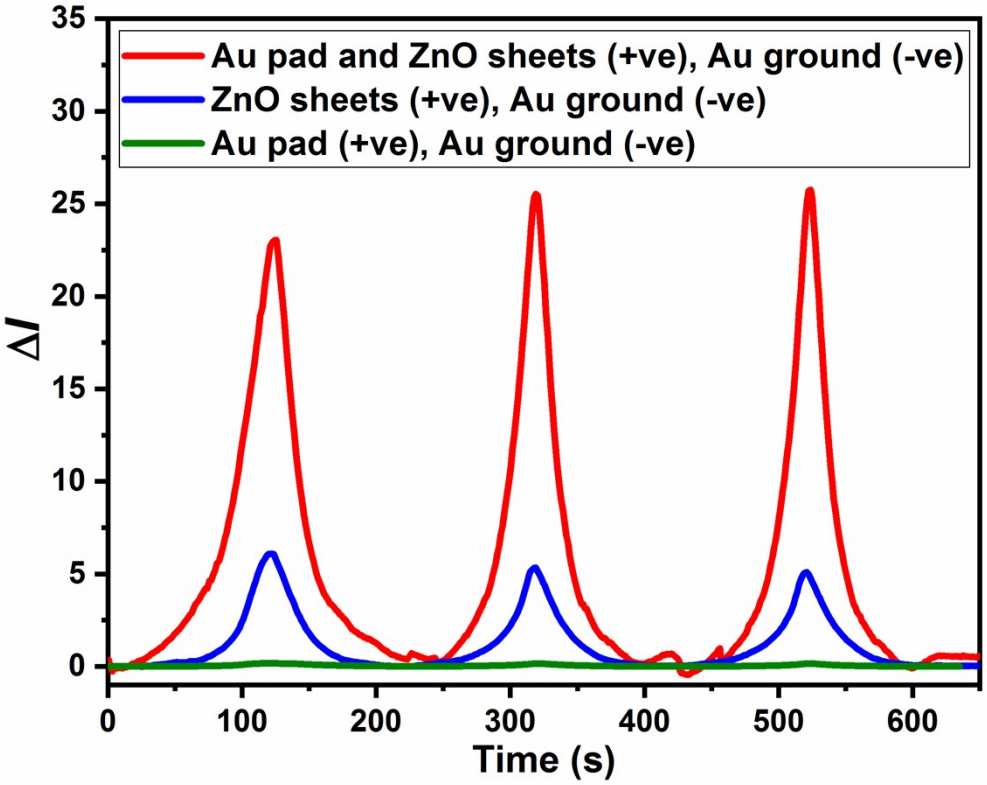

Fig. S10. Change in current (ΔI) for plain $MAPbI_3$ with different circuits after initial poling at 1.5 V/μm for 5 min with a maximum 37 kPa pressure under 0.1 sun illumination in air. The red curve shows the total current modulations in the device, blue curve represents the current modulations only through the ZnO layer and the green curve displays the current modulations through only the perovskite layer.

We observed a higher change in current, when both the Au pad and ZnO sheets on ITO are positive and Au ground is negative. This is attributed to overall more electron extraction by Au and ZnO sheets. In contrast, when the ZnO sheets on ITO is positive and Au ground is negative; ΔI is less because in this case only the ZnO sheets can extract the electron. While in the case where the Au pad is positive and Au ground is negative, the pressing of ZnO sheets on $MAPbI_3$ will not make any difference in current.

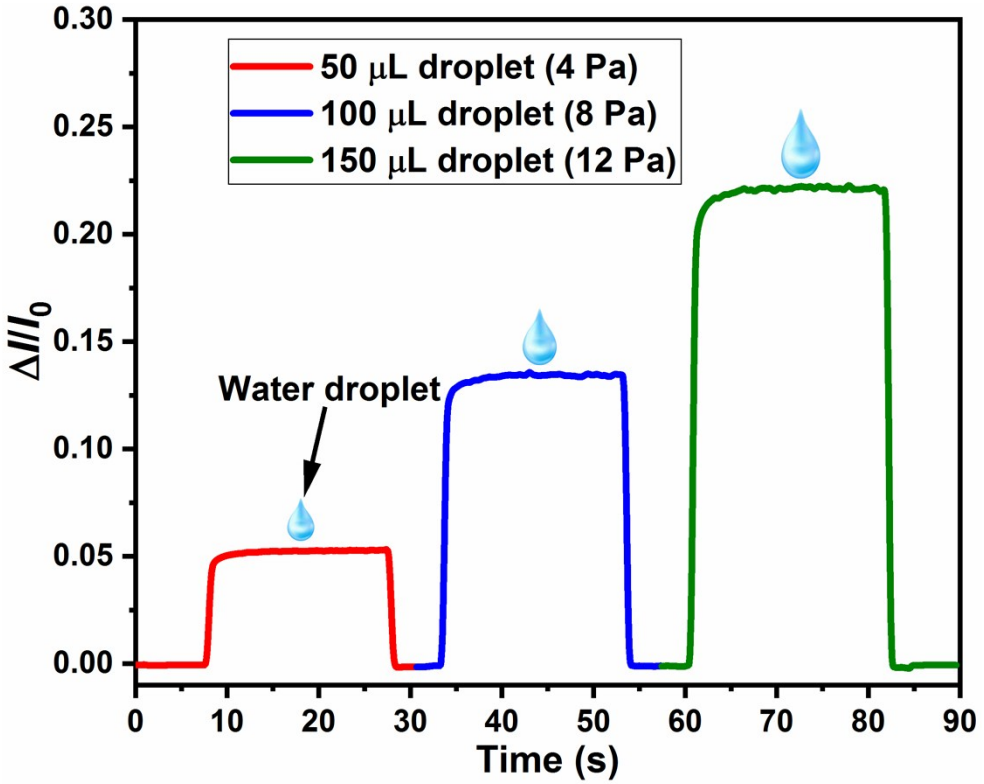

Fig. S11. Minimum pressure limit of detection for the 1 wt % PS-$MAPbI_3$ sensor.

The 1 wt % PS-$MAPbI_3$ device once poled at 5 V/μm for 5 min can sense the pressure changes due to placing of small water droplets. On placing the 50 μL water droplet on the device which corresponds to an extremely low static pressure of 4 Pa, the relative current increased from 0 to 0.05 and it reverts to original level on removing the 50 μL droplet. Further on increasing the volume of the water droplets from 50 μL (4 Pa) to 150 μL (12 Pa), the relative current also increases from 0.05 to 0.22. The device also tracks the removal of the droplets. There is no significant noise in the signals even at ultralow pressure regime which signifies the stable operation of the device.

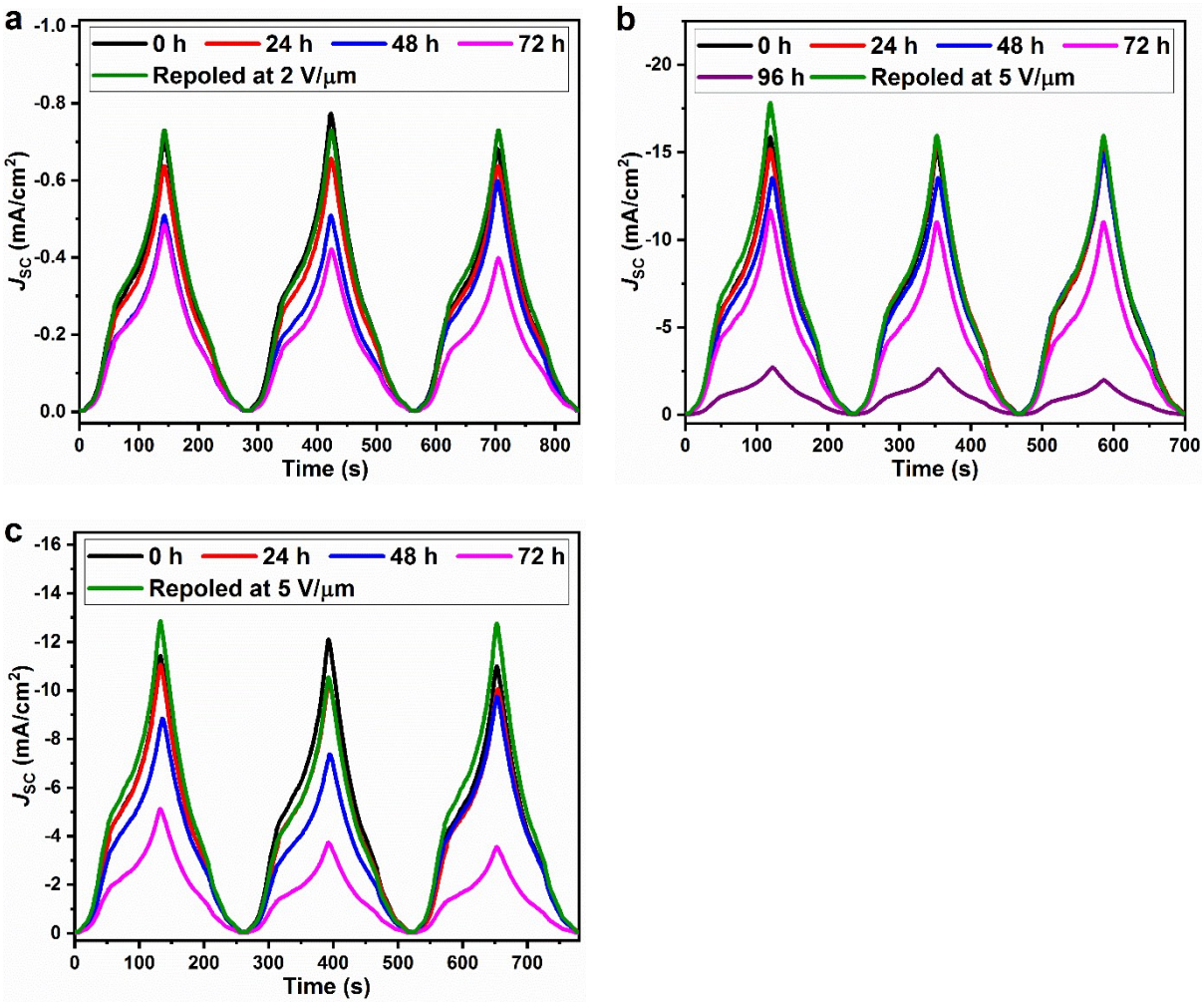

Fig. S12. Self-powered operation of a) Plain $MAPbI_3$, b) 3 wt % PS-$MAPbI_3$, and c) 7 wt % PS-$MAPbI_3$ pressure sensors.

At maximum poling fields of 2 V/μm, the J_{sc} response from plain $MAPbI_3$ devices to load cycles of 111 kPa is maintained for almost 48 h. Afterwards, the J_{sc} decreased to half of its initial value for 72 h. We observed the decrease in the base J_{sc} (at base pressure) with time, which relates to the loss of poling. But the device can be repoled to recover its performance and can be reused again. Similarly, the 3 wt % and 7 wt % PS-$MAPbI_3$ devices once poled at 5 V/μm field can easily function for 72 h and 48 h, respectively without an active power source.

Table S1. Comparison of the operating voltage, dynamic pressure range, linear sensing response, and sensitivity of different reported pressure sensors.

Sensing principle	Key material	Operating voltage (V)	Pressure range (kPa)	Linearity	Sensitivity (kPa^{-1})	Ref.
Transistor	ZnO nanosheets and PS-$MAPbI_3$	Self-powered	0.004 – 450	Linear	20	This work
Transistor	Printed SWCNT active-matrix backplane	10	1 – 20	Linear	8	[24]
Transistor	Silver nanowires embedded PDMS electrode	1	0.0009 – 6.6	Linear upto 0.6 kPa	9.9 (<0.6 kPa)–0.6 (0.6–6.6 kPa)	[25]
Transistor	Indium-gallium-zinc oxide and polyurethane	4	5 – 50	Linear	43.6 (50 kPa)	[26]
Transistor	Graphene with air-dielectric layers	25	0.25 – 3000	Linear upto 500 kPa	2.05×10^{-4} (<500 kPa)–9.43×10^{-6} (500–3000 kPa)	[27]
Transistor	Microstructured PDMS and PII2T-Si	200	0.03 – 55	Linear upto 8 kPa	8.2 (<8 kPa)–0.38 (30–55 kPa)	[28]
Transistor	Graphene and ion gel	2	5 – 40	Linear	0.12	[29]
Piezoresistive	Ultrathin gold nanowires	1.5	0.013 – 5	Linear	1.14	[30]
Piezoresistive	Graphene–polyurethane sponge	1	0.009 – 10	Linear upto 2 kPa	0.26 (<2 kPa), 0.03 (2–10 kPa)	[31]
Piezoresistive	SWNT and PDMS	2	0.0006 – 1.2	Linear upto 0.3 kPa	1.8 (<0.3 kPa)	[32]
Piezoresistive	Pt-coated polymer nanofibres	0.5	0.003 – 1.5	Linear	11.45	[33]
Piezoresistive	Hollow-sphere polypyrrole structure	–	0.0008 – 100	Linear	7.7 (0.1 kPa), 0.4 (1 kPa), 0.004 (100 kPa)	[34]
Piezoresistive	rGO and PDMS microstructure	–	0.016 – 40	Linear upto 2.6 kPa	25.1 (<2.6 kPa), 0.45 (2.6–40	[35]

					kPa)	
Piezoresistive	Laser-scribed graphene	–	5 – 113	Nonlinear	0.96 (<50 kPa), 0.005 (50–113 kPa)	[36]
Piezoresistive	CNT–composite elastomers	10	0.0002 – 59	Linear upto 0.5 kPa	15.1 (<0.5 kPa)	[37]
Piezoresistive	Multilayer Microdome-patterned rGO/PVDF composite	–	0.0013 – 353	Linear	47.7	[38]
Piezoelectric	Micropattern PDMS structures and Ag nanowires	Self-powered	0.0021 – 13	Linear upto 3.2 kPa	0.31 (<3.2 kPa), 0.01 (3.2–13 kPa)	[13]
Piezoelectric	PDMS and PAAm-LiCl hydrogel	Self-powered	1.3 – 101.2	Linear upto 70 kPa	0.013 (<70 kPa)	[14]
Capacitive	Microstructure-d PDMS	80	0.003 – 7	Linear upto 2 kPa	0.55 (<2 kPa)–0.15 (2–7 kPa)	[39]
Capacitive	Ecoflex dielectric layer and Ag electrode	–	0.0073 – 360	Linear upto 16 kPa	0.0224 (<16 kPa), 0.00125 (16–360 kPa)	[40]
Capacitive	Single-layer graphene	–	0.11 – 80	Linear upto 20 kPa	0.0093 (<20 kPa)– 0.0077 (60–80 kPa)	[41]
Capacitive	Graphene	–	0.5 – 450	Nonlinear	0.002	[42]
Capacitive	Carbon Nanotube and Ecoflex	–	0.00016 – 130	Linear upto 5 kPa	0.601 (<5 kPa), 0.077 (30-130 kPa)	[43]
Capacitive	Carbon nanotubes	–	50 – 900	Linear	0.23×10^{-3}	[44]

References

1 W. C. Oliver and G. M. Pharr, *J. Mater. Res.*, 2004, **19**, 3–20.